Construction, Testing, and Characterization of Vertical Drift Chambers for Qweak

A thesis submitted in partial fulfillment of the requirement
for the degree of Bachelor of Science with Honors in
Physics from the College of William and Mary in Virginia,

by

Douglas C. Dean III

Accepted for Honors

Advisor: Prof. David S. Armstrong

Prof. Gina L. Hoatson

Prof. Todd D. Averett

Prof. Robert M. Lewis

Williamsburg, Virginia
May 2009

Contents

Acknowledgments **iii**

List of Figures **v**

List of Tables **vi**

Abstract **v**

1 Introduction **1**

2 The Q_{weak} Experiment **3**

2.1 Overview of Q_{weak} 3

2.2 Physics of Q_{weak} 4

2.2.1 Parity 6

2.2.2 Asymmetry 7

2.3 Design of Q_{weak} 7

2.4 Tracking System 10

2.4.1 Drift Chambers 11

2.4.2 Vertical Drift Chambers 13

3 Construction of Vertical Drift Chamber **16**

4 Testing of the Vertical Drift Chamber **24**

4.0.3 Overview 24
4.0.4 Gas Handling System Testing 24
4.0.5 High Voltage Testing and Conditioning 26
4.0.6 Chamber Efficiency Testing 37
4.1 Conclusions and Future Plans 50

Acknowledgments

I would like to thank Professor Armstrong his time and patience that he has given me. This project would have been very difficult without his constant help. Also, I would like to thank John Leckey for his explanations that helped me better understand key concepts of this project.

List of Figures

2.1 Running of $\sin^2\theta_W$ 5

2.2 Parity Transformation 6

2.3 Q_{weak} Experimental Setup 8

2.4 Q_{weak} Beamline Path through Setup 9

2.5 Vertical Drift Chamber Mounting 11

2.6 Cross Section of Vertical Drift Chamber 14

2.7 Electric Field Lines of VDC 15

3.1 Layers of VDC Chamber 17

3.2 Layout of Chamber 17

3.3 Seperate Components of G10 Frame 18

3.4 Completed G10 Frame 19

3.5 High Voltage Frame 19

3.6 Lab Table Used for Making G10 Frames 20

3.7 Tin Coated Copper Strips Around Outside of HV Frame 21

3.8 Wire Frame 21

3.9 Sketch of the Gas Handling System Used for VDC 22

3.10 Bubbler 23

4.1 Gas Handling System Connections 27

4.2 Grounding Sense Wires for High Voltage Testing 28

4.3 Plot of Initial Conditioning of Chamber 31
4.4 Log Plot of Initial Conditioning of Chamber 32
4.5 Evidence of Arcing Within the Chamber 34
4.6 Garfield Simulation without Missing Wire 35
4.7 Garfield Simulation with Missing Wire 36
4.8 Different Current vs. Voltage Plots Made During Conditioning 37
4.9 Log Plot of Current vs. Voltage During Conditioning 38
4.10 NIM Module Setup Used for Measuring Efficiency 39
4.11 Plot of Initial Efficiency of Chamber 42
4.12 Logic Diagram for Electronics of Efficiency Testing 44
4.13 Timing Diagram for Electronics of Efficience Testing 45
4.14 Efficiency Setup with MAD Card 46
4.15 Plot of Final Measurements of Efficiency 48
4.16 Copper Shielding Used on MAD card 49
4.17 Plot of Current Being Drawn From Indiviual Wire Cards 51

List of Tables

4.1 Initial Conditioning of Chamber 30

4.2 Conditioning of Chamber After Time 33

4.3 Initial Efficiency of Chamber using ^{90}Sr Source Without 2^{nd} Readout Card 41

4.4 Initial Efficiency of Chamber using ^{90}Sr Source With 2^{nd} Readout Card 41

4.5 Efficency Testing with ^{90}Sr Source 47

4.6 Efficency Testing with Cosmic Rays 47

Abstract

Q_{weak} is an experiment set to take place at Jefferson Lab that will put the Standard Model to the test by measuring the weak charge of the proton by precisely measuring the parity-violating asymmetry of elastic proton-electron scattering. Vertical Drift Chambers, which will momentum analyze events that take place, will be key to the tracking system of Q_{weak}. A vertical drift chamber was constructed and conditioned by applying high voltage to the chamber. After conditioning, the current that the chamber would draw at 3.55kV began to spike to 10.3μA and therefore we were cautious to go above this voltage level when testing the chamber. The efficiency of the chamber was measured using cosmic rays and a ^{90}Sr source. Using cosmic rays, the efficiency of the chamber was (95.3 $\pm$ 1.3)% at 3.5kV, whereas when using the ^{90}Sr source, the efficiency of the chamber was (81.3 $\pm$ 1.9)% at 3.5kV. However, it was discovered that these efficiencies were contaminated by background noise that was being picked up by the electronic equipment used to measure the efficiency. After eliminating this background noise, the efficiency of the chamber was again measured, yet it was not at an operating efficiency, which is typically on the order of 99 - 100%. It appeared that the chamber needed to be able to handle larger voltages, however, this was not possible due to the amount of current that the chamber would draw at these larger voltages. It was discovered that the bottom wire frame was the source of the current at these large voltages, so we decided to disassemble the chamber and replace this wire frame. The chamber was then reassembled and is currently being conditioned.

Chapter 1

Introduction

The Standard Model of Particle Physics was developed in the 1970's as a means to connect the electromagnetic, strong and weak interactions, yet, the theory is viewed as incomplete because it does not correctly account for the gravitational force. Although the Standard Model has correctly predicted what has been observed by experiments, there is reason to believe that the Standard Model is not "the" model for particle physics. One of the major inconsistencies with the Standard Model is that it contains many free parameters. Ideally, a unifying theory tries to minimize free parameters, yet, the Standard Model contains as many as 17 free parameters. The mysterious Higgs Boson, which is predicted by the Standard Model, has yet to be discovered although many experiments have been designed to find it. (However, one explanation why the Higgs may have not been discovered yet could be that the mass of the Higgs is above the upper limit of mass for the designed experiments, preventing the Higgs from being detected.) Experiments have also verified that the neutrino has mass, which is inconsistent with the predictions of the Standard Model, which was originally constructed with massless neutrinos. These inconsistencies have raised the question whether there is a physics beyond the Standard Model, creating a need to test the Standard Model. The Q_{weak} experiment seeks to measure the weak charge of the proton, which is firmly predicted by the Standard Model, and therefore will serve

as a test of the Standard Model.

The purpose of this research has been threefold. The first part of this project has been to aid in the completion of a vertical drift chamber that will be used in the Q_{weak} experiment. Drift chambers, which are precision gas-filled wire chambers, will be used in Q_{weak} for the detection of elastically scattered electrons. Much work on building a drift chamber, including the process of how the chamber will be built, had been accomplished before the start of this project, yet, not all components of the chamber had been finished. Also, a gas handling system to monitor the outflow and leak rate of the gas used to pressurize the chamber was designed and built.

The two other components of the research project has consisted of testing the completed drift chamber and analyzing the data collected. High voltage, which is necessary for the operation of a drift chamber, was carefully applied to chamber using a high voltage power supply. Once the chamber had been "conditioned," testing of the efficiency of a single wire was started. For this, cosmic rays and a ^{90}Sr radioactive source was used.

Chapter 2

The Q_{weak} Experiment

2.1 Overview of Q_{weak}

The Q_{weak} experiment will attempt to make an extremely precise measurement of the weak charge of the proton as a means of testing the Standard Model. The weak charge of the proton, Q_W^P, is a measure of the strength of the neutral weak coupling of the proton, analogous to the electric charge for the electromagnetic interaction. In the Standard Model, it is related to the weak mixing angle, θ_W, via

$$Q_W^P = 1 - 4\sin^2\theta_W. \tag{2.1}$$

The experiment will use Thomas Jefferson National Laboratory's (JLab) leading parity-violation facility to measure the parity-violating asymmetry in elastic proton-electron scattering due to the weak interaction at a low momentum transfer. It is required that the experiment be highly precise, with a combined statistical and systematical error of 4%.

The Standard Model predicts the weak charge of the proton based on the "running" of the weak mixing angle $\sin^2\theta_W$. The weak mixing angle is a parameter in the Standard Model that varies as a function of the momentum transfer at which it is probed. In the Standard Model, the weak mixing angle is defined as the ratio of the

masses of the $W^{\pm}$ and Z^0 bosons by

$$cos^2\theta_W = \frac{M^2_{W^{\pm}}}{M^2_{Z^0}} \tag{2.2}$$

and connects the weak interaction to the electromagnetic interaction, i.e. the mixing of these interactions. In any process that a photon can be exchanged, a Z^0 can also be exchanged [1]. At energies and momentum transfers larger than the mass of the Z^0, the Z^0 exchange contributions are comparable to that of photons, and therefore the process that takes place involves both the weak and electromagnetic interactions. The mixing of these interactions is related to the parameter $\sin^2\theta_W$. Figure 2.1 illustrates both the Standard Model's prediction of $\sin^2\theta_W$ as a function of the momentum transfer, Q, and previous measurements of the "running" of $\sin^2\theta_W$. The first of these points, labeled APV, corresponds to an atomic parity violation experiment using ^{137}Cs [6, 9]. The second, $Q_w(e)$, corresponds to a measurement from the parity violating *Møller* experiment [6, 10]. The third, $\nu - DIS$, is a measurement taken from the neutrino/antineutrino scattering from iron [6, 11]. Q_{weak} differs from these other measurements in that it will measure the "running" of $\sin^2\theta_W$ to a much higher precision, which is indicated by the error bars in Figure 2.1. It is key to point out when looking at Figure 2.1 that the measurements of the future experiments are arbitrarily placed on the plot since it can not be sure what these measurements will be.

2.2 Physics of Q_{weak}

The asymmetry in parity-violating elastic proton-electron scattering that Q_{weak} will measure is a result of the weak interaction that takes place between the proton and electron. The weak interaction, which is experienced by quarks and leptons, is carried by three bosons, W^+, W^-, and the Z^0, which all three act differently with

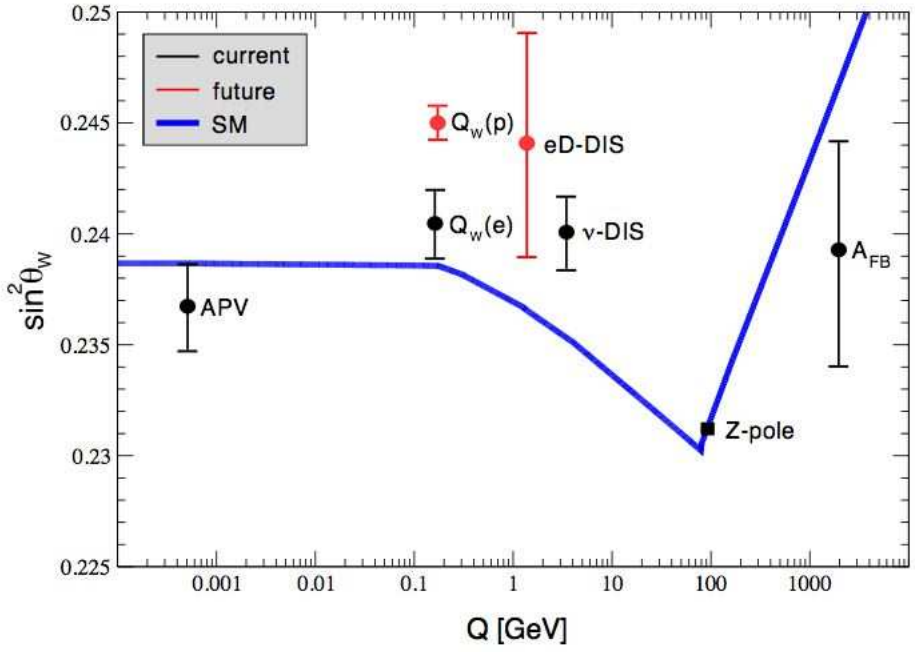

Figure 2.1: This figure illustrates the "running" of $\sin^2\theta_W$ as a function of the momentum transfer Q(GeV/c). SM (blue) represents the Standard Model's prediction. Black points (current) are previous measurements that have been made to date [9, 10, 11]. Red points (future) are future measurements that have been planned. These future points are arbitrarily placed on plot since it can not be sure where these points will fall. However, the error bars indicate the anticipated precision level of the experiment.

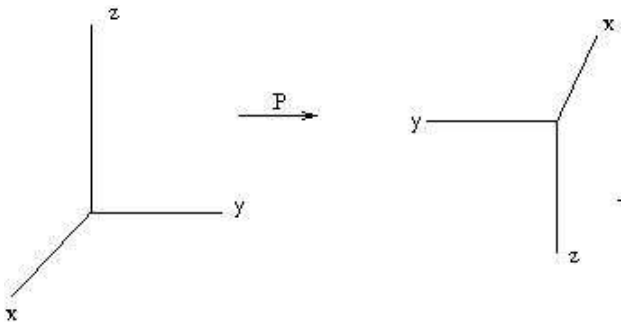

Figure 2.2: This figure illustrates a parity operation acting upon a Cartesian Coordinate System. The parity operation inverts the spatial coordinates of the Cartesian Coordinate System. Notice that the system is transformed from a right handed system to a left handed system.

fermions [1]. Specifically, the W^+ has a charge of +1 and only acts on a fermion that has spin parallel to its velocity (right-handed fermions). The W^- has a charge of -1 and only acts on a fermion that has spin anti-parallel to its velocity (left-handed fermions). The Z^0 is neutral and acts on both right handed and left handed fermions, however it acts on the two types with a different magnitude, creating an asymmetry between the probability for scattering of right-handed and left-handed fermions.

2.2.1 Parity

A parity operation is a spatial inversion which inverts the coordinates of a vector $\vec{r}$ to $-\vec{r}$, and therefore a parity operation acting on a right-handed coordinate system transforms the system into a left-handed coordinate system, as shown in Figure 2.2 [2, 3, 4]. It was originally believed that the laws of physics were invariant under a parity operation, meaning that one could not tell the difference between right and left-handed systems. However, in 1956, Lee and Yang predicted that parity might be violated in weak interactions which was confirmed experimentally using the beta decay of ^{60}Co soon after by Wu et al. [2].

2.2.2 Asymmetry

The asymmetry that is created by the parity-violating elastic proton-electron scattering is defined by

$$A \equiv \frac{\sigma^+ - \sigma^+}{\sigma^+ + \sigma^-}, \tag{2.3}$$

where σ^+ is represents the the scattering cross section of the fermions that are right handed and σ^- represents the scattering cross section of the fermions that are left handed. By applying Quantum Field Theory, one can also show that the asymmetry is proportional to the weak charge of the proton [5], given by

$$A = \frac{1}{P}\frac{-G_F}{4\pi\alpha\sqrt{2}}[Q^2 Q_W^P + Q^4 B(Q^2)]. \tag{2.4}$$

This equation is a low order approximation of the asymmetry, with P representing the polarization of the electron beam, Q^2 representing the 4-momentum transfer, G_F representing the Fermi coupling and α is the fine structure constant. Higher-order terms, (arising from hadronic structure effects, such as gluons), are represented by $Q^4 B(Q^2)$ and can be ignored at low momentum transfers. Thus, at a low momentum transfer, by measuring the asymmetry in the elastic proton-electron scattering, the measurement of the weak charge of the proton can be made, which is how Q_{weak} will measure the weak charge of the proton.

2.3 Design of Q_{weak}

A schematic of the experimental setup for Q_{weak} can be seen in Figure 2.3. It will use a 1.165GeV, 85% polarized electron beam that is incident on a 35cm liquid hydrogen target. The beam will pass through a double collimator that will select out the electrons that have scattered from the target at $9^\circ \pm 2^\circ$. This scattering angle is consistent with an acceptable momentum transfer of $Q^2 = 0.03(\frac{GeV}{c})^2$. A toroidal magnet will then bend the elastically scattered electrons away from the beamline and

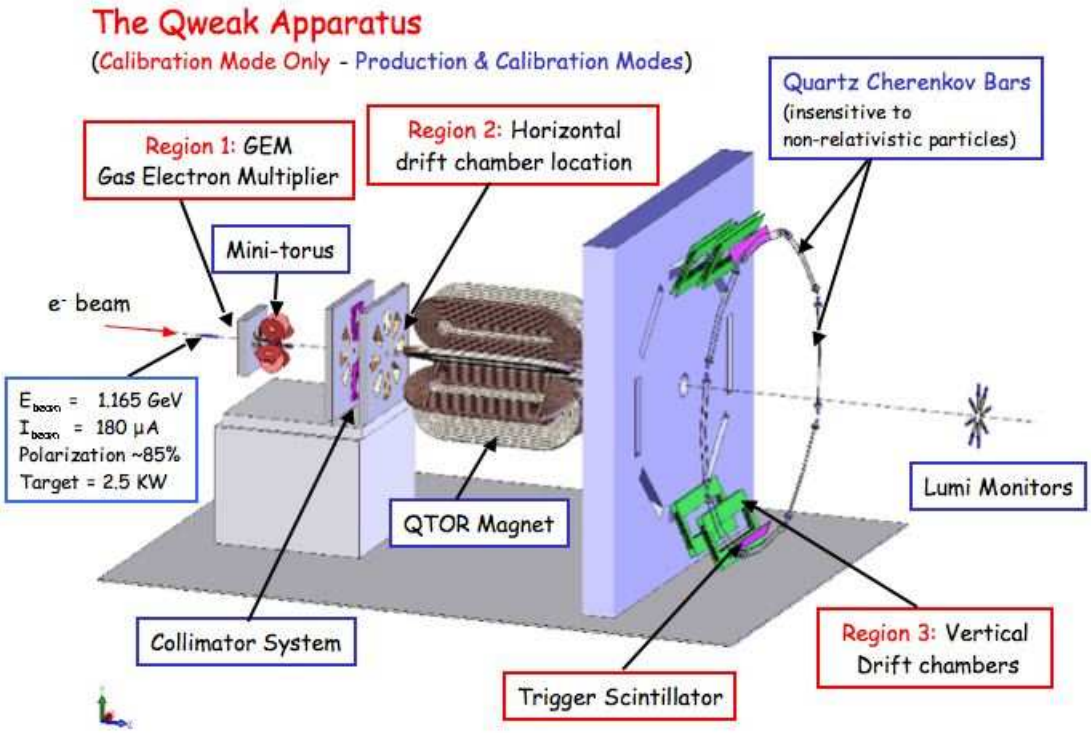

Figure 2.3: The tracking system for Q_{weak} will consist of 3 different regions. Region 3 is composed of the Vertical Drift Chambers that the William and Mary group is responsible for providing. Čerenkov detectors will be used to measure the asymmetry in the elastic proton-electron scattering.

focus them on to the plane of Čerenkov detectors, Figure 2.4 [6, 7]. These Čerenkov detectors are similar to a scintillator in that it will emit a small burst of light once an electron is detected. Using photomultiplier tubes, the signals that come from the Čerenkov detectors will be converted to a current signal and then read out to a computer. In order to measure the asymmetry of parity-violating elastic proton-electron scattering, this will be done for both right-handed and left-handed electrons by changing the polarity of the incident electron beam.

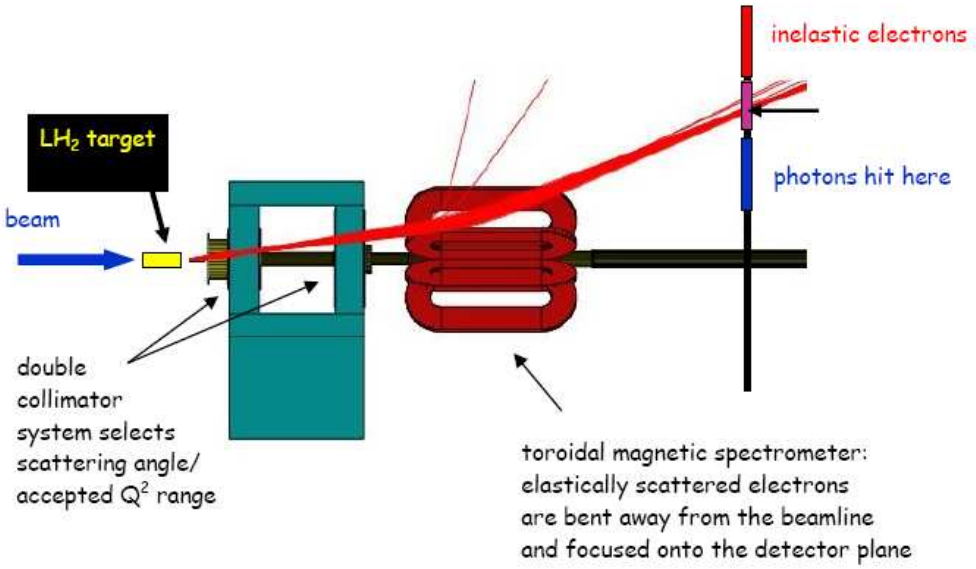

Figure 2.4: This figure illustrates the path that the beamline takes as it passes through the experimental setup of Q_{weak}. The beamline is incident on a liquid hydrogen target and then passes through a precision collimator that selects out the electrons with a particular scattering angle. The toroidal magnet then bends the elastically scattered electrons away from the beamline to the Čerenkov detectors.

2.4 Tracking System

A tracking system, consisting of three different regions, will be used periodically to make subsidising measurements of the momentum transfer, Q^2 [6]. For elastic scattering, the momentum transfer is given by

$$Q^2 = \frac{4E^2 sin^2\frac{\theta}{2}}{1 + 2\frac{E}{M} sin^2\frac{\theta}{2}}, \tag{2.5}$$

where E is the incident electron energy, θ the scattering angle and M the proton mass. Hence, knowing the incident electron energy and the scattering angle, the measurement of the momentum transfer can be made. The incident electron energy will be determined with $\leq$0.1% precision using the Hall C energy measurement system [6]. The collimator that will be used will allow for a precision measurement of the scattering angle of the elastically scattered electrons.

However, to ensure the electrons that were detected by the Čerenkov detectors were indeed elastically scattered from the proton target, the tracking system will also allow for the recreation of the electron's path or track. The beam current will be turned down from 180μA to approximately 10pA because the large beam current would destroy the chambers used during the tracking. Region 1 will determine the location of the elastically scattered electrons as they emerge from the collimator. Region 2 will determine the position of the scattered electrons right before they enter the toroidal magnet. Hence, the spatial distance between Region 1 and Region 2 will define the scattering angle that the elastically scattered electrons traverse before entering the magnet [6]. Region 3 will consist of two Vertical Drift Chambers (VDC's) and will momentum-analyze events in order to ensure that the electrons that enter the Čerenkov detectors were indeed elastically scattered. These chambers will determine the trajectories, measuring position and angle, of events that take place, from which

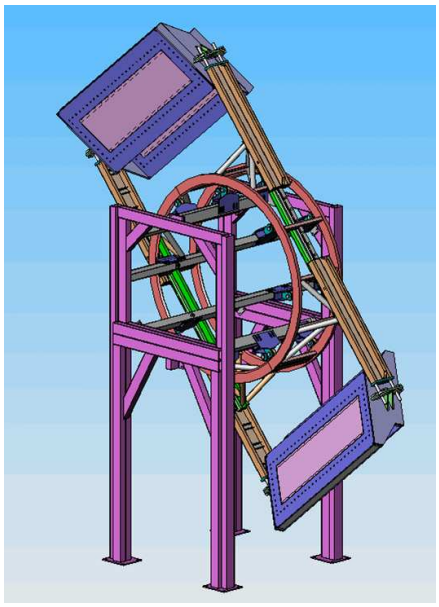

Figure 2.5: Chambers are placed at opposing octants so that two measurements can be made at a time. A total of 4 measurements will need to be made in order to cover the entire detector system.

a measurement of the momentum can be made.

The William and Mary group has taken up the design and construction of the Region 3 Vertical Drift Chambers. These chambers will be mounted to rotating wheel (Ferris wheel design) that will allow for measurements in two opposing octants. See Figure 2.5. Thus a total of four separate measurements will be needed in order to cover the entire detector system. These types of measurements will be made approximately every few weeks during a 2-year-long data-taking process.

2.4.1 Drift Chambers

Drift chambers are gas-filled devices that contain an array of wires and use a high electric field to detect charged particles. For purposes of Q_{weak}, the Region 3 vertical drift chambers will be used to determine the location and angle of the

primary electron after the magnetic field resulting from the elastic proton-electron scattering. Wires are spaced approximately 5mm apart from one another and are held at ground, while high voltage is applied to the chamber in order to generate a large electric field within the chamber. The velocity of an electron as it traverses through the chamber is determined by the type of gas mixture that is used. Previous experiments that used vertical drift chambers have used an Argon/Ethane mixture inside their chambers. This mixture has unique properties in that the drift velocity of an electron is relatively constant. However, it has not been decided if this gas mixture or another (such as Argon/CO_2/Methane, which will be used in testing the vertical drift chambers) will be used for Q_{weak}. Although the electrons accelerate due to the electric field, they collide with the gas molecules causing them to slow down. This process of accelerating and colliding with gas molecules continues until the electron reaches a wire within the chamber, and results in a constant drift velocity.

As an electron passes through the chamber and collides with the gas, it ionizes the gas within the chamber (primary ionization), producing more electrons and ions that are accelerated by the large electric field. As a result of the electric field, these primary electrons drift towards the anode wires. However, the electric field, E, at the wires is very large and so when the primary electron drifts near a wire, it undergoes a large acceleration causing a build up of ionization around the wire; this is known as the avalanche effect. The electrons trigger the sense wires upon which a signal is sent out to the data collecting electronics that are attached to the chamber. The drift time, the time that elapses for the first electron to trigger a wire, along with the drift velocity is used to determine the distance travelled by the electron that triggered the wire. Knowing several of these drift distances for several wires in the chamber can be used to determine the track of the primary scattered electron.

2.4.2 Vertical Drift Chambers

Vertical Drift Chambers (VDCs) are a type of drift chamber that tracks the primary electron by triggering on ionization that has travelled in the vertical direction. Figure 2.6 shows the operating principle of a Vertical Drift Chamber that will be used for Q_{weak}. As described, when the primary electron enters the chamber, it ionizes the gas producing more electrons that drift in a vertical direction due to how the electric field is applied to the chamber. Negative high voltage will be applied to the chambers in order to generate the large electric fields needed to accelerate the electrons. Therefore, ions that are created will drift to cathode planes while the primary electrons will drift towards the anode-sense wires of the chamber, which are held at ground. The drift time of these events is determined and since the drift velocity of the particles is relatively constant (due to the acceleration and collisions with the gas) the drift distances of the electrons can be computed. By knowing this drift distance, since these electrons "drifted" in the vertical direction, one can trace backwards to determine where the primary scattered electron was located in the chamber. This process can be repeated for multiple primary electrons that resulted from the scattered electron and a track of the scattered electron can be generated.

However, the electrons do not drift in a true vertical direction because the electric field lines, near the wires, are not truly vertical (see Figure 2.7 [7]). The reconstruction of the track of this scattered electron can be made more accurately with the use of a drift chamber simulation software known as GARFIELD [6, 7, 12]. This program models the electric field within a drift chamber, allowing one to see the electric field lines of a drift chamber's particular setup. GARFIELD simulates the drift of the electrons inside the chamber and therefore allows one to determine a functional relationship between the time of arrival of the first drift electron at the wire

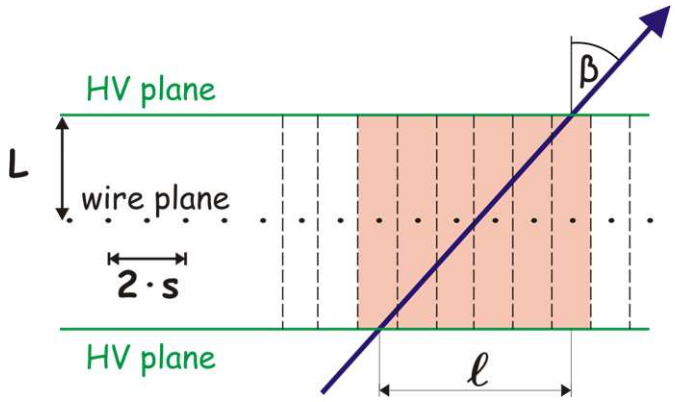

Figure 2.6: A cross section of a Vertical Drift Chamber that will be used in Q_{weak}. The top and bottom lines are the high voltage planes that create the large electric fields within the chamber. The black dots through the center is a plane of the wires used to detect the ionized electrons. The region highlighted in red is the region that could be triggered by ionized electrons that result from the incoming track. L represents the the distance from the top of the plane to the wire plane, ℓ represents the length along the chamber from where the primary electron first enters the chamber and exits the chamber. β is the angle of the incoming electron.

and the perpendicular distance to the location of the primary electron. By knowing this perpendicular distance, one can extrapolate from the sense wire to determine the location at which the primary scattered electron. This process is repeated for multiple wires in order to reconstruct a single track. With this reconstructed track and the track information from Regions 1 and 2, and by studying the light output of the Čerenkov detectors as a function of the location/angle of the incident track, experimenters are able to determine if the scattered electron resulted from an elastic or inelastic event.

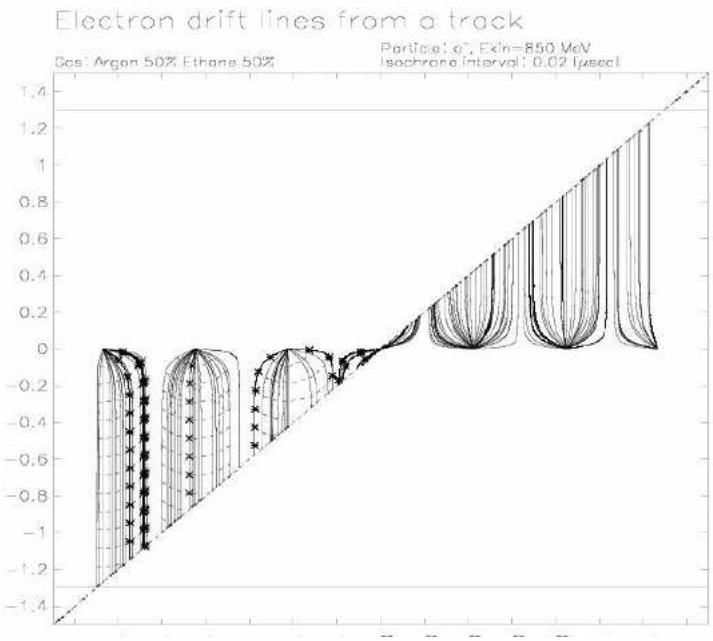

Figure 2.7: This figure illustrates the electric field lines within a Vertical Drift Chamber as a result of a GARFIELD simulation. As one can see, the electric field lines near a wire are not vertical, and therefore the path of an electron near a wire is not going to be in the vertical direction. Avalanche amplification is of the order 10^6 and occurs in the regions near the wires. With GARFIELD, one is able to better determine where the drift electron resulted from, causing the reconstructed track to be more accurate.

Chapter 3

Construction of Vertical Drift Chamber

The William and Mary group has been working on the construction of these vertical drift chambers, being extremely precise and careful in their steps to build the chamber. Overall, the group will need to build a total of 5 of these drift chambers, which 4 (2 in each octant) will be used at one time and the extra will serve as a backup. The chamber itself is a sandwich of eight customized G10 boards that are held in place by large aluminum frames, Figure 3.1. G10 is a fiberglass material that is made out of a special glass epoxy, which is extremely strong. G10 was decided to be used because it was durable enough to support the large size that the chamber would be, but also it is electrically neutral, so that it would not interfere with the electric field within the chamber. Between the aluminum frames there are three high voltage planes, which are used to create the large electric field needed inside the chamber to accelerate the ionized electrons, two wire frames, two gas frames and 1 spacer frame, Figure 3.2. The purpose of the wire frame is to support the sense wires that will be used to read out the signals from inside the chamber. The tensions of each wire and the relative spacing between wires need to relatively uniform in order to maintain precise measurements of the drift time. The gas frame allows for the inflow and outflow of the gas mixture used inside the chamber.

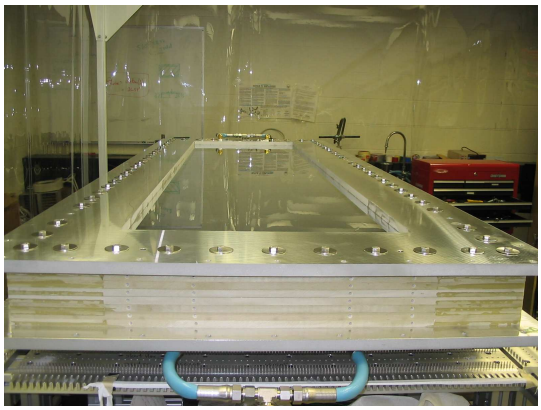

Figure 3.1: This photo shows the different layers of the Vertical Drift Chamber. The chamber is held together by two large aluminum sheets that are bolted together with the rest of the layers. The chamber is composed of 3 high voltage frames (foil frames), 2 wire frames, 2 gas frames and 1 spacer frame.

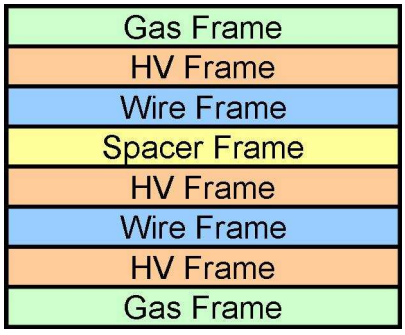

Figure 3.2: This figure illustrates the layout for the Vertical Drift Chamber. Large aluminum sheets (not pictured here) will be used to sandwich the different layers together and held in place using nuts and bolts

Figure 3.3: This photo illustrates the 4 different components that the G10 frames were constructed out of. These four components were epoxied and clamped together to create the G10 frame.

The G10 frames were constructed from four separate pieces which were epoxied together, Figure 3.3 and 3.4. In order to ensure this connection would hold, each corner of the frames were clamped down until the epoxy set. The G10 frames also needed to be cleaned very well using acetone in order to ensure that dirt or dust particles would interfere with measurements inside the chamber. For the high voltage and gas frames (Figure 3.5), a conductive aluminized mylar foil was stretched across the G10 using a specifically designed lab table (Figure 3.6) and then epoxied in place. The purpose of the mylar is to hold the high voltage potential to create the large electric field needed inside the chamber. In order to ensure an electrical connection between the mylar and high voltage potential that would generate the electric field, a strip of tin-coated copper strips were placed inside a machined groove around the perimeter of the frame and held in place using a conductive epoxy, Figure 3.7. The wire frames (Figure 3.8) were carefully made using 25μm gold-plated tungston wire, with each frame containing 280 wires. Each frame was then again cleaned and stored away so that dust and other dirt particles would not penetrate the chamber.

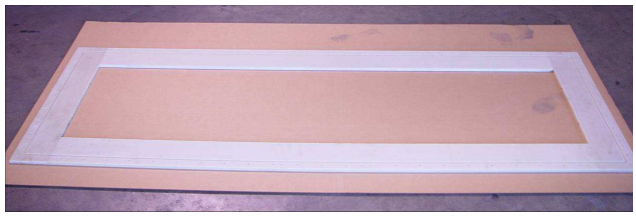

Figure 3.4: This photo illustrates a typical completed G10 frame after the G10 components had been epoxied and clamped.

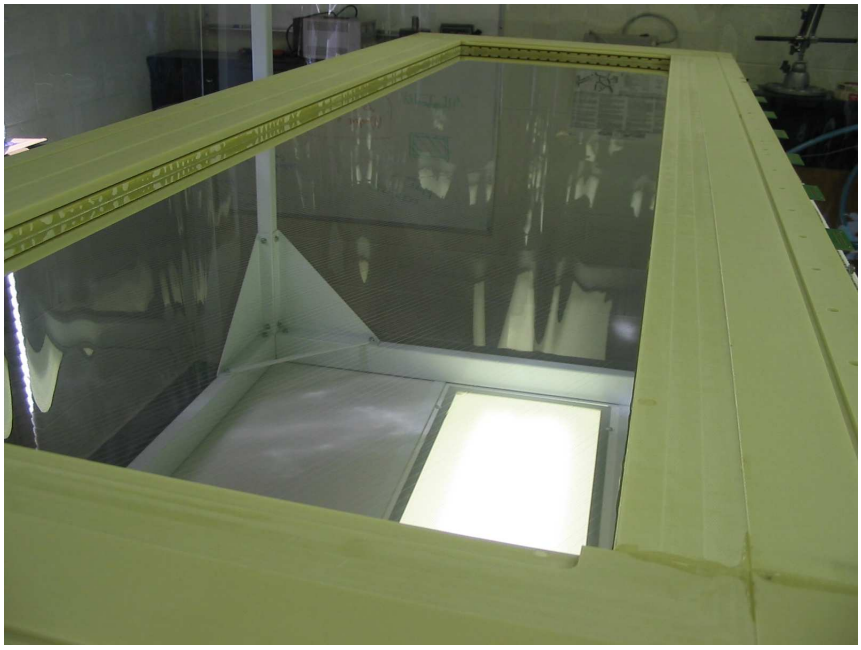

Figure 3.5: This photo shows the spacer frame positioned on top of a completed high voltage (HV) frame that will be used in the Vertical Drift Chamber. High voltage will be applied to the mylar in order to create a large electric field within the chamber that will be used to create ionization.

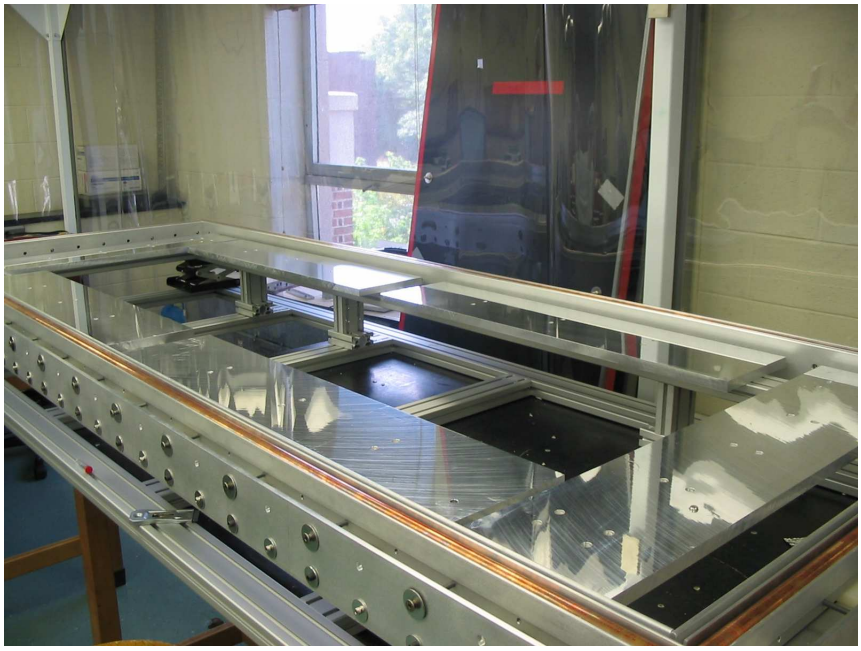

Figure 3.6: This photo illustrates the lab table that was used to stretch the mylar foil across the high voltage (foil) frames and the gas frames. The table was designed with a U-groove around the outside edge, with a copper pipe that sits in this groove. For a frame, a piece of mylar the size of the table was cut. The edges of the mylar were then taped and wrapped around the copper pipe until it was tight. The U-groove was then displaced from the table, using the screws that attached the U-groove to the table, until the mylar was stretched tight with no visible wrinkles. Testing the tension of the mylar was done by gently pushing down with a hand. It was not necessary that the tensions in the different foils all be exactly the same.

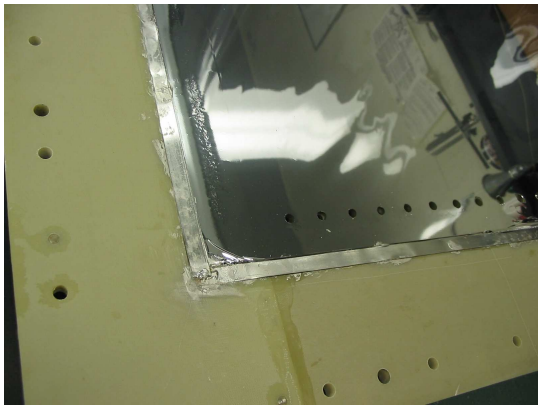

Figure 3.7: This photo shows the tin coated copper strip that lays along the outside of the HV frame. This strip is used in order to ensure a electrical connection between the high voltage and the mylar foil.

Figure 3.8: This figure is a "zoomed in" image of a completed wire frame that will be used inside the VDC. The wire is 25μm in diameter, making it extremely sensitive and difficult to work with. The wires are held in place using an epoxy. This epoxy was made from AY 103 resin and HY 991 hardener that had to be mixed together. Once epoxied in place, the epoxy needed to cure for 12 hours.

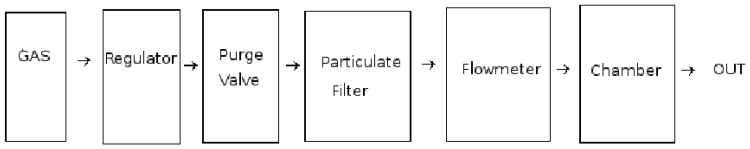

Figure 3.9: This is a sketch of the gas handling system that was designed to deliver the gas mixture to the VDC. The gas travels from the source into a pressure meter (or flow meter in this case) so that the inflow can be monitored. It then enters the chamber and exits through a bubbler. The bubbler does not allow any gas to flow back into the chamber.

Once all the different frames had been completed being built, the next step in the process was designing a bubbler system that would allow the gas mixture to flow in and out of the chamber, without any other gas flowing back in. It is crucial for the operation of the chamber that no other gas but the mixture be inside the chamber because this can affect the ionization rate. It was also necessary to be able to monitor the flow of the gas in and out of the chamber in order to get a "leak rate", or be able to estimate what the leak rate of the chamber may be. The solution that was devised was a gas handling system, see Figure 3.9. This system would allow for the measurement of the inflow of the gas mixture by using a flow meter right before the entrance of the chamber. However, the most important component of the gas handling system is the bubbler, Figure 3.10. Gas from the chamber "bubbles" through a liquid (mineral oil) that is inside the bubbler and then is vented outside. The gas is not able to flow back into the chamber because it can not penetrate the mineral oil. The physical system was constructed from Swagelok connectors and gas hoses while the flow meters were purchased from Airgas.

The final stage in the construction process was assembling the chamber. This entailed stacking the different frames on top of one another in the correct order as

Figure 3.10: This photo shows the bubbler that was constructed for the gas handling system. Gas from the chamber enters the bubbler and then "bubbles" through a thin layer of mineral oil. Since the gas can not penetrate the mineral oil, it is vented out through another tube due to the pressure that builds up inside.

previously shown, 3.2. Extreme care and patience was needed in the assembly because the wires on the wire frames could be easily broken. Also, in order to create a seal within the chamber to prevent gas from leaking out, O-rings were used along each different layer. These also needed to be throughly cleaned and glued in place. The large aluminum sheets were used to sandwich the 8 different layers together. Bolts and nuts were then fastened tightly using a torque wrench to finish the construction of the chamber. Although care was taken, while installing the lower wire frame, one of the wires did break. In order to get a chamber assembled as quickly as possible, this wire was not initially reattached.

Chapter 4

Testing of the Vertical Drift Chamber

4.0.3 Overview

In order to see if the constructed chamber would operate properly, tests on the chamber were next performed. Testing of the vertical drift chambers was done in multiple steps, each step testing different components of the chamber. By testing parts of the chamber, malfunctioning components could be pinpointed and repaired, while operating parts could be verified that they were indeed functioning properly. Testing was done in a three stage process as follows: First, the gas handling system was tested to make sure that the gas would be effectively delivered to the chamber. Next, high voltage was applied to the chamber in order to see if the chamber could handle the voltage. Finally, using cosmic rays and a ^{90}Sr beta source, detection of tracks as well as the efficiencies of individual wires inside the chamber were tested.

4.0.4 Gas Handling System Testing

Overview

Testing of the gas handling system was important because it is vital that the correct, pure gas mixture be inside the chamber during operation. Therefore, it needed to verified that the bubbler was working properly and that no other gas

was getting inside the chamber. For example, O_2 can "poison" the operation of the chamber. Also, it was necessary to estimate a leak rate for the chamber to have an idea about how much gas was escaping from the chamber. The leak rate will be important for the main experiment because the gas mixture that will be used contains ethane, and due to safety regulations at Jefferson Lab, a value (or estimate) of how much gas escapes from the chamber should be known.

Testing Setup

To test the gas handling system as well as measure the leak rate of the chamber, the chamber was connected to the gas handling system via the Swagelok connections (Figure 4.1) which in return was connected to the Argon/Carbon Dioxide/Methane (88%/10%/2%) mixture that would be used for testing. A regulator was connected to the bottle containing the gas mixture so that the pressure of the bottle and the outflow pressure could be monitored. Connected to the regulator was an (Y40-LF1728) Airgas particle filter that filters out 100% of particles larger than 0.003μm that may be inside the bottle of gas. An Airgas flowmeter was connected in series between the chamber and the gas regulator and was used to monitor the gas flow into the chamber. Once the system was connected, the gas was then turned on, upon which it filled the chamber. It was observed that the gas from inside the chamber would bubble out through the bubbler, however the bubbling rate was not at all constant. The cause for this, we hypothesize, is due to a threshold pressure that the chamber must overcome to bubble through the mineral oil that is inside the bubbler.

Results from Testing Bubbler

The leak rate for the chamber was determined to be approximately $0\frac{\ell}{hr}$. This was computed by observing the rate at which the bubbler would bubble as gas flowed through the chamber. While gas is flowing through the chamber, it was noticed that

the aluminumized mylar that keeps the gas inside the chamber would expand and contract. This was associated with a "breathing" effect that existed as a result of the threshold pressure for the bubbler. Once the pressure inside the chamber met this threshold, the chamber would "exhale" or expel the gas mixture through the bubbler. Below this threshold, the bubbler would not bubble. It was observed that with a flow rate of $21\frac{\ell}{hr}$, the bubbler would bubble for 7 minutes and be off for 9 minutes. Repeating this with a flow rate of $29\frac{\ell}{hr}$ it was observed that the bubbler would bubble for 14 minutes and then be off for 6 minutes. The difference in volume due to the expansion and contraction of the aluminum mylar was determined to be approximately 3 liters (out of a total volume of 111ℓ) by calculating the amount of gas that flowed into the chamber during the time that the bubbler was not bubbling. Once the bubbler stopped bubbling, the flow rate was then set to $2\frac{\ell}{hr}$ and it was observed that the bubbler again bubbled in approximately 1.5 hours. Therefore, 3 liters of gas was delivered to the chamber ($2\frac{\ell}{hr}$ * 1.5 hours) and since the difference in volume due to the expansion and contraction of the mylar was 3 liters, very little gas leaked from the chamber. A precise measurement of the leak rate of the chamber was not necessary and so we concluded that the leak rate was approximately $0\frac{\ell}{hr}$. Similarily designed vertical drift chambers, used by Hall A at Jefferson Lab, had a leak rate of $3\frac{\ell}{hr}$ for 48ℓ chambers.

4.0.5 High Voltage Testing and Conditioning

Overview

The next part to testing the VDC was applying the high voltage that would be used to generate the electric fields inside the chamber. The expected outcome of these tests was to identify the voltage range that the drift chamber would require in order to operate properly. This voltage would be determined by making a plot of the

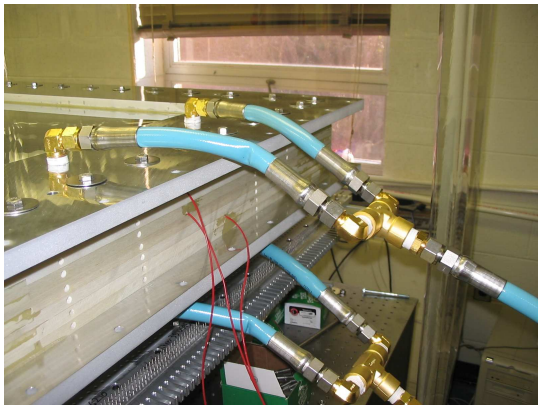

Figure 4.1: This photo illustrates the connections from the gas handling system to the vertical drift chamber. All the connections were done using Swagelok connectors. Connections stemmed from the Argon/Carbon Dioxide/Methane mixture, to a flow meter (which monitored the input flow), to the chamber and then out through the bubbler (which was exhausted outdoors through a window).

high voltage versus the current drawn by the chambers. As the voltage is increased, the current drawn by the chamber increases until the chamber reaches a particultar operation region. While in this region, the current levels off with increasing voltage. The voltage associated with this plateau is the voltage range that is required for the operation of the chamber. When increasing the voltage pass this range, the current drawn from the chamber again increases. The plateau region of the chamber is the region in which the chamber is most efficient, and therefore is the region in which it should be operated.

High Voltage Setup

In order to place high voltage on the chamber, the sense wires needed to be grounded and so it was necessary to devise a way to do this. The wires, which are connected to the readout cards on the chamber, needed to be grounded because during the actual experiment the wires will be placed at ground but also because this would stop them from charging up when raising the voltage on the chamber. To

Figure 4.2: This figure illustrates how the readout cards and therefore the sense wires were grounded while applying high voltage to the drift chamber. Small aluminum rods were soldered to each DIN pin connector and then wires were soldered to each of the aluminum rods. The aluminum rods were connected to one another using a grounding wire. The end of the grounding wire was then taped on to the aluminum frame to ensure a ground connection.

ground the wires, $\frac{1}{8}$" aluminum rods were soldered on to the DIN pin connectors that attach to the readout cards. Wires were then soldered to each of the aluminum rods, which were then connected to a grounding wire. This grounding wire connected all the readout cards to one another, Figure 4.2. The end of the grounding wire was then connected to the aluminum frame of the chamber via a piece of electrical tape, creating a common ground.

A transition box that would take the safe high voltage (SHV) connection from the high voltage (HV) power supply to the chamber also needed to be made. The high voltage is generated from a single channel of a Bertan negative high voltage (model 377N) power supply. The output from the power supply was ran through an RC protection circuit that used a 1MΩ resistor and 330pF capacitor. This protection circuit prevents any large spikes in current that could occur when increasing the voltage on the chamber to large values. This output was then connected to 3 silicone-coated

high voltage wires, (called SIL-KOAT, 500 feet spool) each of which are connected to the cathode planes of the drift chamber. The diameter of the wire is 2mm and was chosen because it is rated to a maximum of 20kV with no corona discharge.

Results from Testing and Conditioning

Once the sense wires were grounded and the transition box in place, the voltage was turned on. First, only 100 V was placed on the chamber so that a multimeter could be used to check that the sense wires and outer aluminum frames of the chamber were properly grounded. The voltage was then slowly increased. To ensure the safety of the chamber, the trip setpoint was set to 100μA scale. This trip setpoint acts similar to an adjustable breaker box in that the voltage is "tripped" when the current exceeds 80% of the setpoint limit. (In this case, the trip setpoint was set at the 100μA scale, the circuit would trip if the current being drawn reached 80μA.) The first trip occurred at a voltage of 1.1kV. These trips are associated with "training" the drift chamber. In training a chamber, dust particles and other dirt is burned off as the voltage is ramped up and the chamber "learns" how to handle higher voltages. During the beginning stages of training the chamber, the voltage and quiescent currents were recorded, Tables 4.1 and 4.2.

It was observed that the current increased as the voltage on the chamber increased. However, the difference between these two tables is that the data from Table 4.2 was observed after a longer period of time had elapsed with the voltage on the chamber. During this time, the voltage did not trip off and remained steady. It was observed that for the lower voltages (2.0kV - 2.7kV), the currents drawn by the chamber had decreased with respect to the currents in Table 4.1. This decrease corresponds to the conditioning of the drift chamber. This data supports the idea that as time elapsed with voltage applied to the chamber, more dust and other debris that

could cause corona discharge, sparking or arcing (and therefore current to be drawn) inside the chamber were burned off causing the decrease in current. Since the current levels were decreased by this conditioning, larger voltages were able to be applied to the chamber. Again, this process of leaving the voltage on the chamber for a period of time and allowing for conditioning was repeated for these larger voltages.

Voltage (kV)	Current (μA)
1.9	0.02 $\pm$ 0.001
2.0	0.04 $\pm$ 0.001
2.1	0.09 $\pm$ 0.002
2.2	0.16 $\pm$ 0.005
2.3	0.23 $\pm$ 0.008
2.4	0.32 $\pm$ 0.01
2.5	0.42 $\pm$ 0.015
2.6	0.50 $\pm$ 0.02
2.7	0.78 $\pm$ 0.023

Table 4.1: During the training of the drift chamber, voltages and the associated current at that voltage were recorded. As the voltage is increased, the current on the drift chamber increases, however, there should be a point at which the current begins to level off with increasing voltage. This is known as the plateau and is also the operating region of the drift chamber. After the plateau region, the current again increases with increases in voltage.

Although conditioning had been observed, when raising the voltage on the chamber to a value of 3.35kV the current drawn by the chamber was initially 14μA. The chamber was left at this voltage for a period of 24 hours in the hope of lowering the current. However, after the 24 hours, the current increased to 17μA, and therefore the chamber did not seem to be conditioning any further. However, as one can see from Figure 4.3 and Figure 4.4, the plateau region had not been reached and so the chamber needed to be able to support larger voltages. In order to determine where on the chamber the current was being drawn, an ammeter was used to read the current passing through each of the readout cards. It was found that 95% of the current being

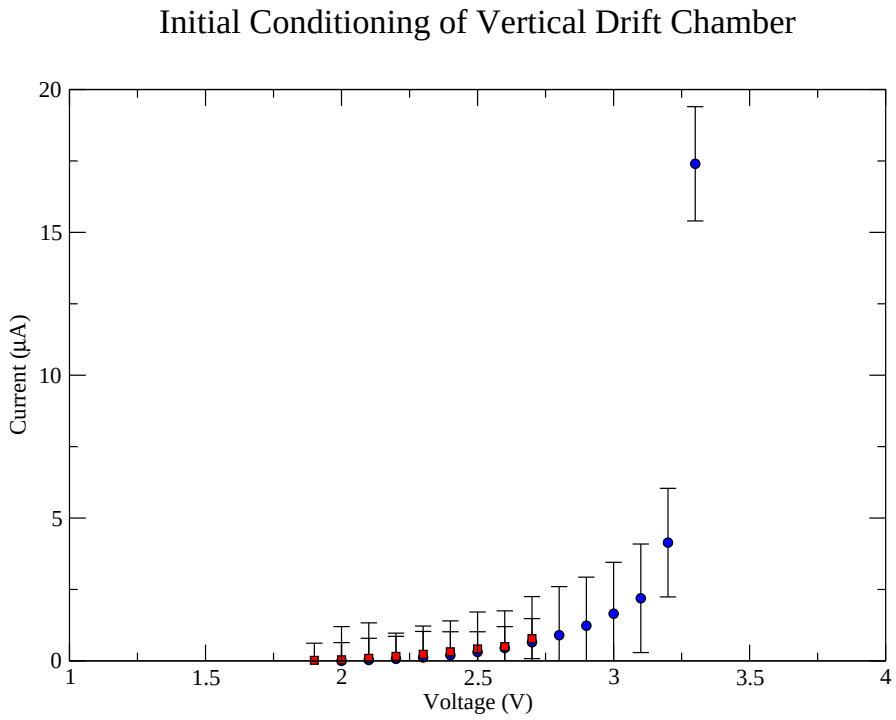

Figure 4.3: This plot shows the initial conditioning of the drift chamber. The blue points are values that were first obtained before allowing time to elapse with voltage on the chamber. The red points are values that were later obtained after allowing the voltage to be applied to the chamber for a period of time. Values were unable to be collected for larger voltages initially because the currents being drawn were much too high. However, there is evidence of some coniditioning since the currents seem to have decreased after allowing voltage to be applied to the chamber. The error bars on the plot were determined by watching the current oscillate using an ammeter while a particular voltage was applied.

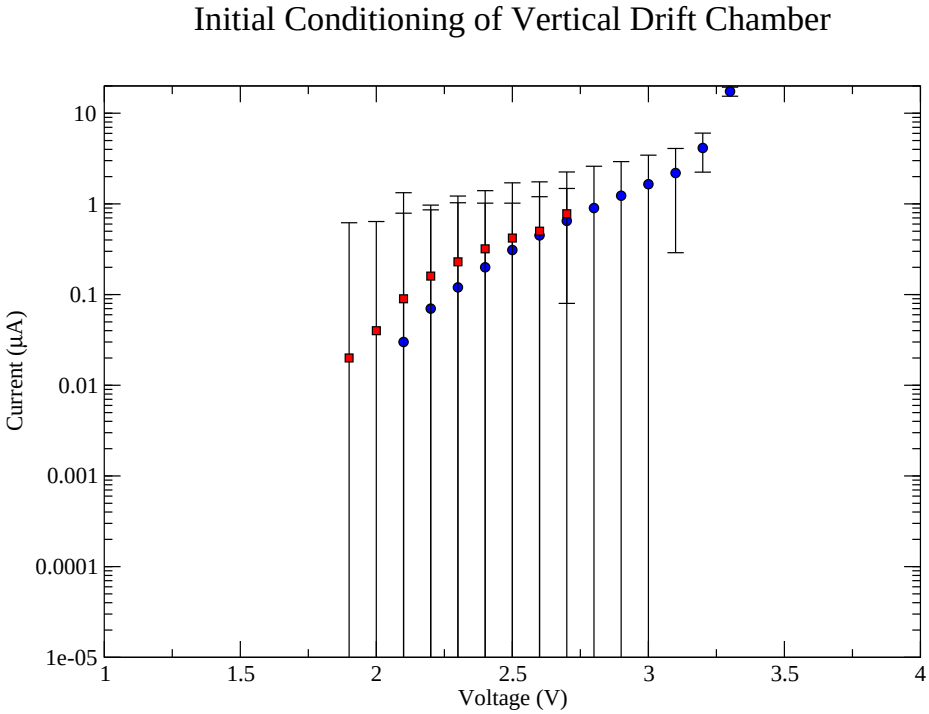

Figure 4.4: This log plot shows the initial conditioning of the drift chamber. The blue points are values that were first obtained before allowing time to elapse with voltage on the chamber. The red points are values that were later obtained after allowing the voltage to be applied to the chamber for a period of time. There is evidence of a plateau in the current (operating region) around 3.4kV.

Voltage (kV)	Current (μA)
2.0	0.00 ± 0
2.1	0.03 ± 0.001
2.2	0.07 ± 0.003
2.3	0.12 ± 0.004
2.4	0.20 ± 0.007
2.5	0.31 ± 0.011
2.6	0.45 ± 0.013
2.7	0.65 ± 0.017
2.8	0.90 ± 0.021
2.9	1.23 ± 0.029
3.0	1.65 ± 0.031
3.1	2.19 ± 0.054
3.2	4.14 ± 0.071
3.3	17.4 ± 2.23

Table 4.2: The voltage was left on the chamber for approximately 8 hours before this data was collected. The voltage did not trip off during this period of conditioning. It was observed that the currents associated with lower voltages decreased with respect to the values of current from Table 4.1. This supports the notion that the chamber was undergoing a conditioning process. Since the current decreased, higher voltages were able to be applied to the chamber. These voltages corresponded with large currents being drawn.

drawn was coming from the adjacent wires on the right and left of the single wire that had broken during assembly. In order to fix this, the chamber was disassembled and the missing wire was replaced. With the chamber apart, spots were observed on the aluminum mylar, Figure 4.5, which is evidence that arcing within the chamber had occured when applying high voltage.

The chamber was reassembled and testing high voltage on the chamber resumed. With the wire replaced, the current that the chamber was drawing when a voltage of 3.35 kV was applied was now at 0.52μA. This was a significant change in current that was observed with the wire missing (17μA). In order to "see" what was happening inside the chamber with a missing wire, a GARFIELD simulation was ran with and

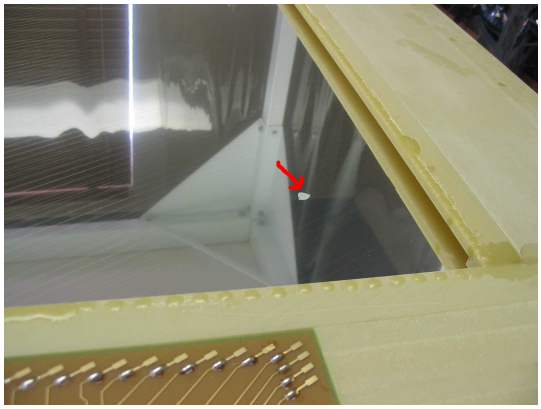

Figure 4.5: The red arrow in the figure illustrates the type of spot that was noticed when the chamber was taken apart. This spot is evidence that the chamber did experience arcing inside when high voltage was applied. This arcing is most likely a result of conditioning.

without a missing wire (Figure 4.6 and Figure 4.7). In comparing these two figures, it became clear that the missing wire had an effect on the electric field inside the chamber. With the wire missing, the electric field was larger in the area between the two adjacent wires, which for purposes of the chamber, was causing larger currents to be drawn. The chamber sat with a voltage of 3.35kV approximately for 48 hours and it was observed that the current decreased to 0.23μA. Again, this was evidence that the chamber was still in the process of conditioning.

The process of conditioning the chamber continued until it was believed that applying higher voltages to the chamber had no effect on the overall dark current. Values of the currents that were drawn at certain voltages were recorded and plots of the current versus the voltage were made. However, these plots seemed to not be changing,(see Figure 4.8) and so it was believed that the conditioning of the chamber was complete. Analyzing these graphs, it was estimated that the currents flattened out around 3.4kV and therefore expected that the plateau region be around this voltage (see Figure 4.9). However, the operating region for the chamber could not be

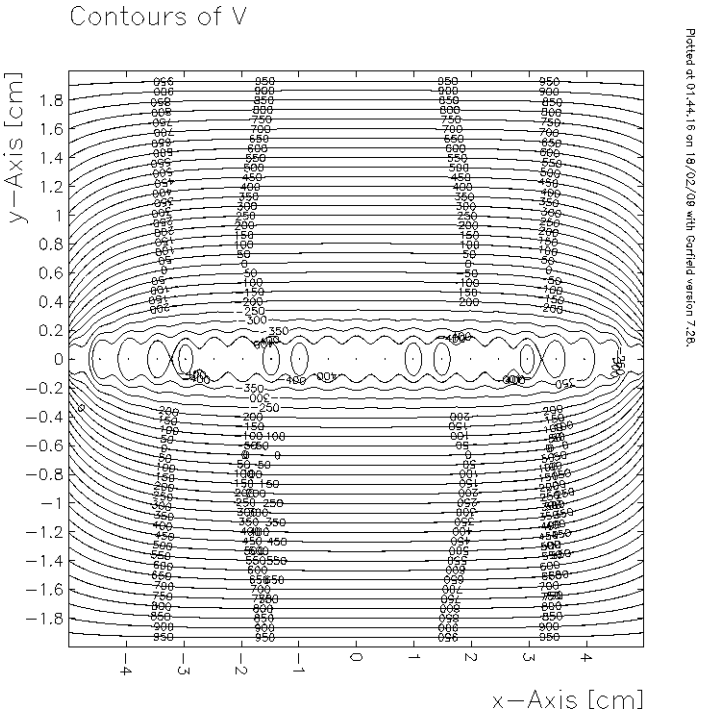

Figure 4.6: This Garfield Simulation illustrates the equipotentials of the drift chamber without a missing wire. There are 21 wires in the x-z plane and 2 infinite planes in this simulation. The infinite planes are at the y = 2cm and y = -2cm coordinates and have a voltage of 1000 V. The contours show smooth, uniform electric field lines around the wires, as expected with all the wires present. This figure was made courtesy of Siyuan Yang.

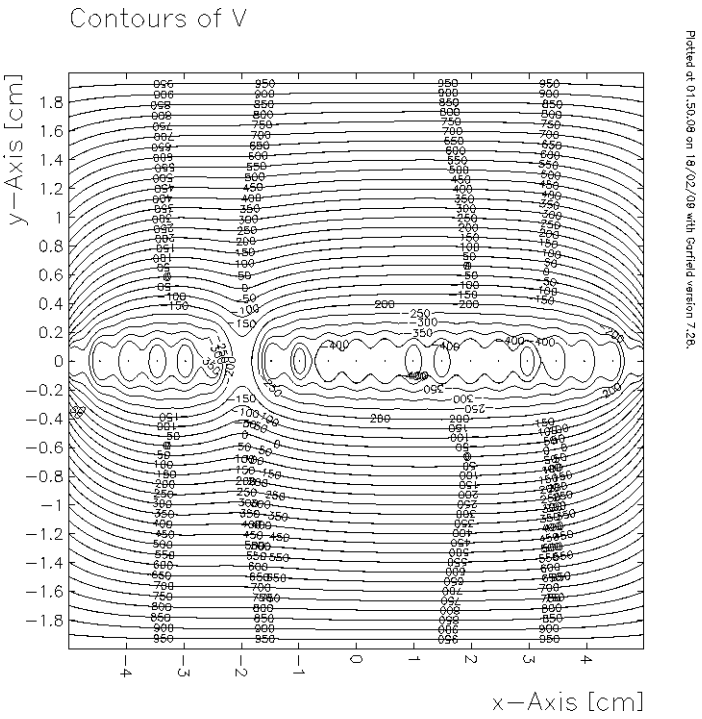

Figure 4.7: This simulation is identical to the simulation in Figure 4.6, except now there is a wire missing at x = -2cm. From this simulation, it is obvious that the missing wire has an effect of the electric field in the chamber, particularly in the area where the wire is missing. The equipotentials are no longer uniform in the location of the missing wire. The gradient of the equipotentials between the two adjacent wires of the missing wire is larger, meaning that the electric field between these wires is larger. This figure was made courtesy of Siyuan Yang.

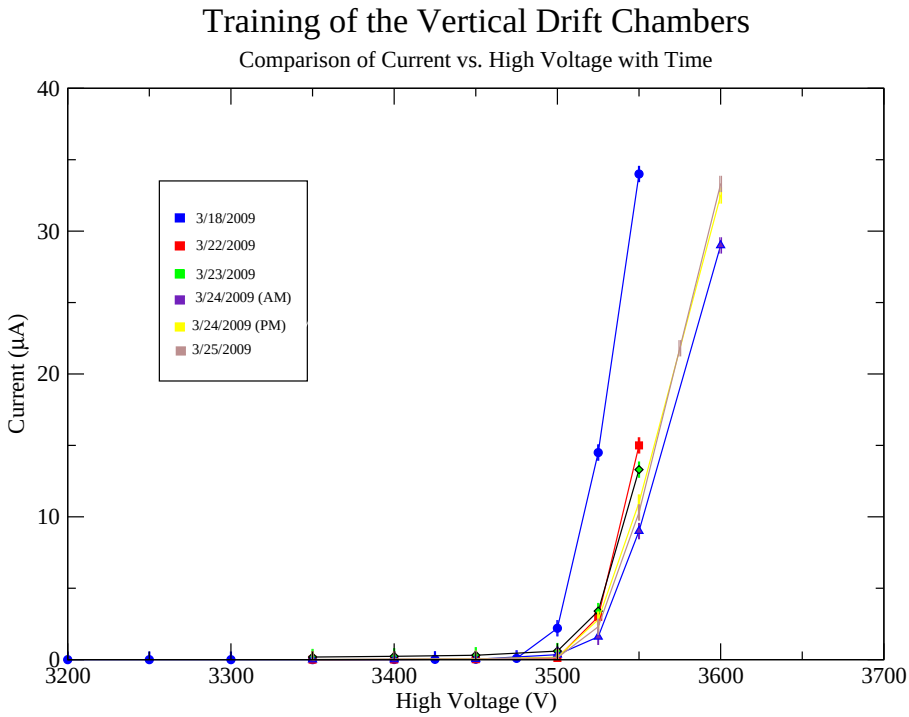

Figure 4.8: This plot shows many of the different current versus voltage graphs that were made during the conditioning of the chamber. It can be seen that the currents do shift towards the right as voltage is increased, showing that the conditioning was happening. However, as time progressed, these plots seemed to be unchanged and therefore it was believed that the conditioning was complete. Also, the last two measurements that were observed, the curve actually shifts in the opposite direction, with high current being drawn at 3550V. The error bars in the figure were determined by the fluctuation in the currents (in the ammeter) as measurements were taken.

identified until actual efficiency measurements were made.

4.0.6 Chamber Efficiency Testing

Overview

The final stage of testing the VDC was measuring the efficiency of the chamber. The efficiency of the chamber is needed to ensure that when a given track passes through the chamber and triggers a wire, the chamber is able to detect that particular track. In order to measure the efficiency cosmic rays and a ^{90}Sr beta source was used.

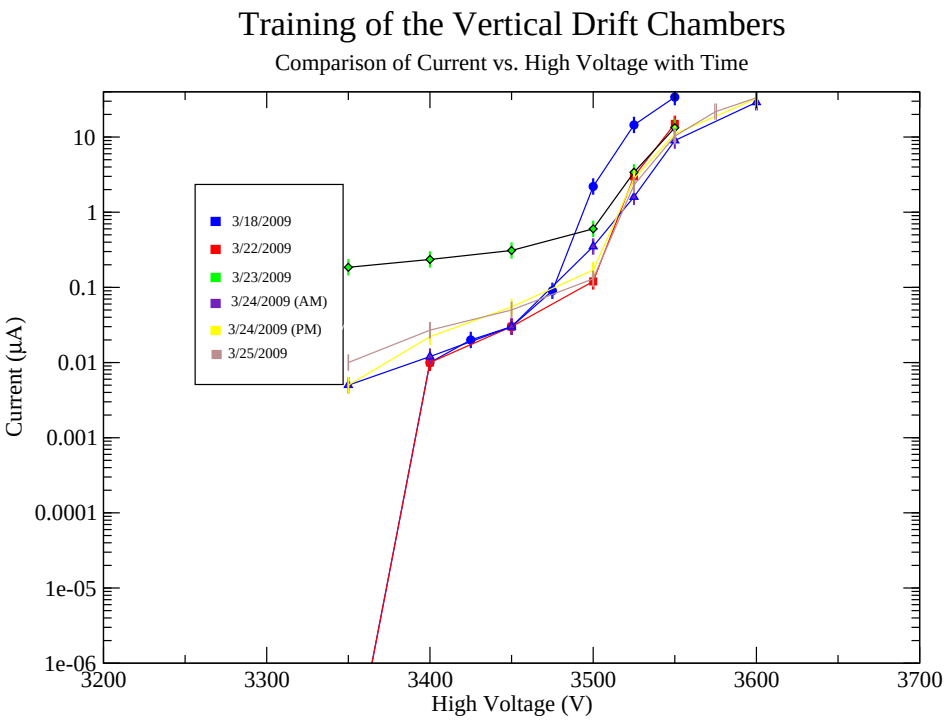

Figure 4.9: This log plot shows many of the different current versus voltage graphs that were made during the conditioning of the chamber. One can see that there is evidence of a plateau region near 3.38-3.4kV. It was believed that voltages near these values correspond to an operating region of the chamber.

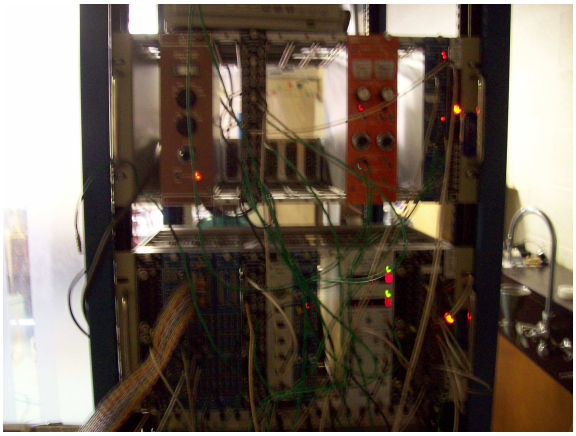

Figure 4.10: This image shows the NIM modules that were used for measuring the efficiency of the drift chamber.

It was expected that as the voltage on the chamber was increased, the efficiency would improve. Also, after having defined a plateau region for the chamber, it was expected that the efficiency of the chamber would be the greatest within this region. To measure the efficiency Nuclear Instrumentation Modules (NIM) were used to analyze the signals detected by the chamber, Figure 4.10.

Initial Testing and Results

A single readout card was selected from the bottom wire plane. The first three wires from this card were selected using alligator clip to BNC cables, with the grounds of the cable being connected to the ground of the frame. The rest of the sense wires from the readout card were grounded. The BNC cable from the 3 wires were then sent to separate channels of a Phillips amplifier module (Model 776) in which the signals were amplified twice, with each stage amplifying by $\times 10$, for a total amplification of 100. This amplification was done so that the electronics would be able to detect small signals. The amplified signal was then sent to NIM (Model 711) discriminators and then to a NIM (Model 754) coincidence module. The purpose of the discriminator

was to allow a 1μs time window to open for each trigger of the wire, whereas the coincidence module allowed for signals that only occurred at the same time to be output. The output from the coincidence module was viewed using a Joerger visual scaler, which counted the number of coincidences. The efficiency of the second wire was tested and defined as the ratio of the coincidences of the all three wires divided by the coincidence of the first and third wire,

$$\text{Efficiency} = \frac{1 \cdot 2 \cdot 3}{1 \cdot 2}, \tag{4.1}$$

where $1 \cdot 2 \cdot 3$ represents connecting wires 1, 2 and 3 in coincidence.

By pointing a ^{90}Sr source at the VDC in the region where the observed wires were positioned, coincidence rates were measured as a function of voltage and these values were recorded, Table 4.3. Values of the current that were drawn from the top cathode plane and the bottom plus the middle cathode planes were also recorded. In order to try to make sure real tracks were being observed, a second readout card was added to the coincidence logic, with all 16 wires from a card on the upper plane added to the coincidence, see Table 4.4. The efficiency with this setup was also recorded and a plot of the observed efficiency was created, Figure 4.11. After using the ^{90}Sr source, and the efficiency of the chamber was left to run using cosmic rays. However, false coincidences (coincidences not associated with either cosmic ray tracks or tracks from the source) were observed. These false triggers were noticed by switching the lights of the lab on and off as well as walking across a clean mat (mat used to take dust/dirt off shoes). It was believed that these false triggers were a result of static charge with was being picked up either by the NIM electronics, BNC cables or sense wires in the chamber. It was observed that the efficiency was strongly correlated to the increasing voltage, as expected. Also, it was noticed that a plateau region may be in the vicinity of 3.38kV, however, voltages above 3.468kV could not be examined

because the current being drawn from the chambers began to spike.

HV (kV)	Threshold (mV)	T Current (μA)	M+B Current (μA)	Efficiency
3.30	700	0.10 ± 0.01	0.27 ± 0.03	No Efficiency
3.35	700	0.13 ± 0.03	0.33 ± 0.04	75 ± 0.04
3.38	700	0.18 ± 0.04	0.41 ± 0.05	92 ± 0.01
3.40	700	0.22 ± 0.04	0.5 ± 0.05	90 ± 0.02
3.40	900	0.23 ± 0.04	0.55 ± 0.05	94 ± 0.008
3.45	500	0.55 ± 0.06	1.0 ± 0.08	88 ± 0.008
3.45	700	0.70 ± 0.08	1.2 ± 0.08	95 ± 0.007
3.45	900	0.58 ± 0.06	1.1 ± 0.08	98 ± 0.006
3.468	700	5.2 ± 0.23	5.4 ± 0.24	96 ± 0.006

Table 4.3: This table shows the data that was collected while testing the efficiency of the chamber with the ^{90}Sr source. "T Current" represents the current that was drawn from the upper foil frame. "M+B" represents the current that was drawn from the middle and bottom foil frames. The threshold in this data represents the threshold at which the NIM discriminator was set. This threshold sets the limit at which the discriminator will fire. One can see that there is a relationship between the voltage on the chamber and the efficiency, as expected. It was also observed that there was a relationship between adjusting the threshold of allowed signals and the efficiency.

HV(V)	Threshold (mV)	T Current (μA)	M+B Current (μA)	Efficiency
3.30	500	0.10 ± 0.01	0.26 ± 0.04	No Efficiency
3.325	500	0.12 ± 0.03	0.31 ± 0.06	55 ± 0.11
3.35	500	0.14 ± 0.03	0.35 ± 0.06	79 ± 0.04
3.40	500	0.23 ± 0.04	0.55 ± 0.07	87 ± 0.02
3.45	500	0.56 ± 0.07	1.1 ± 0.09	93 ± 0.01
3.460	500	2.6 ± 0.11	3.0 ± 0.12	95 ± 0.007

Table 4.4: This table shows the data that was collected while testing the efficiency of the chamber with the ^{90}Sr source while including the coincidence of the top readout card. 'T Current" represents the current that was drawn from the upper foil frame. "M+B" represents the current that was drawn from the middle and bottom foil frames. The threshold in this data represents the threshold at which the NIM discriminator was set. This threshold sets the limit at which the discriminator will fire. One can see that there is a relationship between the voltage on the chamber and the efficiency, as expected. It was also observed that there was a relationship between adjusting the threshold of allowed signals and the efficiency.

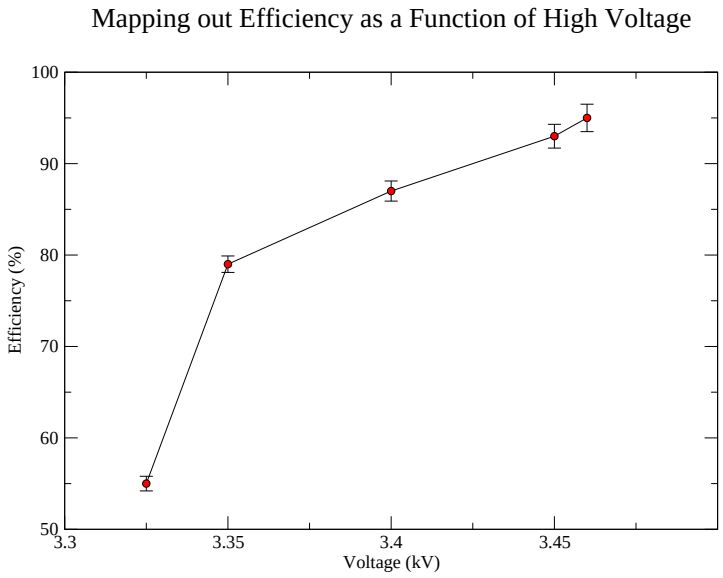

Figure 4.11: This figure is a plot of the measured efficiency of the chamber. From this plot, there is evidence that a plateau may exist around 3.38kV. However, this plot contains very few values and it was also not possible to go above voltages of 4.468kV without the current spiking. Even though the efficiency is not 100% at 3.38kV, the plateau is believed to be in this region and that more precise measurements will need to be measured in order to obtain an efficiency near the expected 100%. However, it is believed that the measurements for this plot contains false triggers, and so the efficiency may be larger than in reality.

Further Chamber Efficiency Testing, Problems and Results

Ideally, the chambers should only detect true cosmic ray tracks, i.e. tracks that travel in a straight line, and propogate through the chamber. However, during the initial phase of testing the efficiency of the chambers, there was concern that the chambers were detecting background noise and cosmic ray events that may not be associated with a single straight track. In order to account for these different events, coincidences were added to the electronics. Scintillators were placed on top of and below the drift chamber, with both signals placed in coincidence with each other. This coincidence was then added to the previous circuit. An antenna was also added as a veto to the coincidences in order to account for the background noise in the lab. The antenna consisted of a BNC to alligator clips cable, with one alligator clip hanging in mid air and the other alligator clip grounded to the frame of the chamber. Figure 4.12 is a logic diagram of the electronics and Figure 4.13 is a timing diagram of the circuit. With the new coincidences added, the measured efficiency was calculated using equation

$$\text{Efficiency} = \frac{1 \cdot 2 \cdot 3 \cdot \text{SCINT}}{1 \cdot 2 \cdot \text{SCINT}}. \tag{4.2}$$

Measurements of the chamber efficiency were again measured at different voltages, but it still remained unclear if the background noise was eliminated with the addition of more inputs into the coincidence logic. It was decided that instead of using BNC to alligator clip cables and NIM amplifier/discriminator for the electronics that the switch to the MAD preamp/discriminator chip [6] be made, Figure 4.14. This particular chip attaches directly to the readout card on the chamber and will be used in the experiment at Jefferson Lab. The advantage of using this card, is that the signals should be less noise-sensitive since the electronics is located right at the readout card and also different wires on a readout card could be monitored at a time.

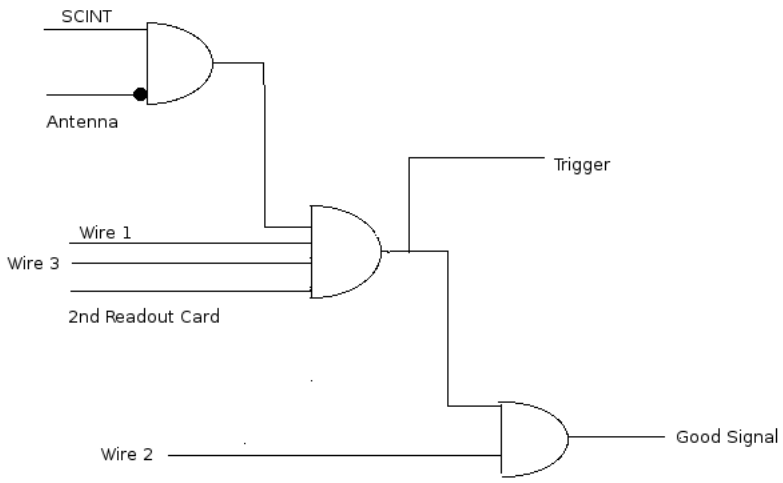

Figure 4.12: This is a simple logic diagram of the setup used to measure the efficiency of the chambers. Coincidence units are represented by AND gates. The "GOOD" output represents a track that was measured by all 3 wires, the second readout card, and the scintillators while the antenna was not being fired. The trigger represents an event in which wires 1 and 3, the second readout card and scintillators coincided, while the antenna was not fired. This trigger represents a track that was not measured by wire 2.

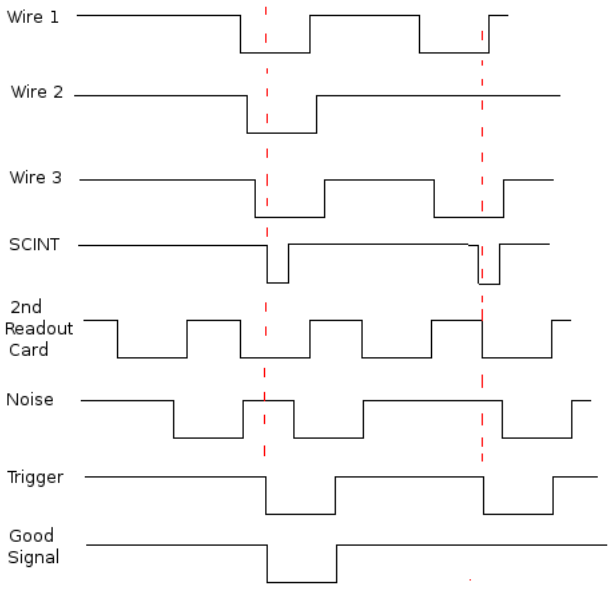

Figure 4.13: This is a timing diagram of the setup used to measure the efficiency of the chamber. The signals from the electronics are discriminated with the output being a 1μs pulse. The scintillators have a discrimated output pulse of 200ns in order to create a small window for the coincidence of events. A measured event occurs if the pulses are fired in the same time window, as indicated. The first dash line represents a good coincidence trigger that results from wires 1,2 and 3 as well as the scintillator firing. The second dash line represents a trigger that results from an inefficient measurement, i.e., wire 2 did not fire when wires 1 and 3 and the scintillator fired.

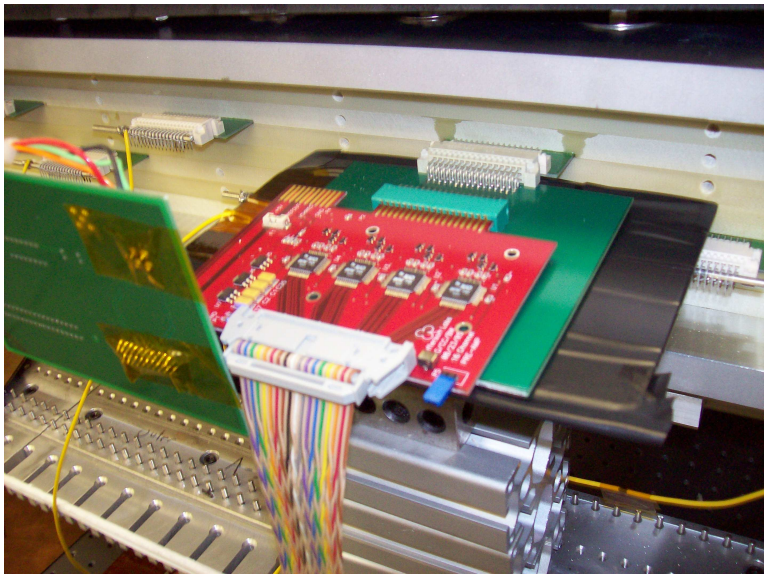

Figure 4.14: This photo illustrates the testing setup including the use of the MAD card. Instead of signals being discriminated using NIM discriminators, the signals were discriminated by the preamp/discriminator of the MAD card. This decreases the chance of picking up noise in the signals and therefore decreases the uncertainty in our measurements.

Emitter coupled logic (ECL) signals from the MAD chip were sent to a Lecroy (Model 4616) ECL to NIM module which converted the signals to a useable NIM logic. The same coincidence circuitry was used as before. In addition to the antenna to take care of noise, a monitor wire, which consisted of a wire further away from the wires that were being observed, was used. The idea behind this monitor wire is that only the 3 sense wires should be fired as a track passes through the chamber. Therefore, if this monitor wire fires in coincidence with the 3 sense wires, it is understood that this event is not a true cosmic track and the signal should be ignored.

Preliminary measurements were made using the MAD preamp/discriminator chip, (see Table 4.5 and Table 4.6) however, it was still unclear whether real events were being observed. These efficiency measurements consisted of data from both cosmic rays and the ^{90}Sr source. The efficiencies were then plotted as a function of

high voltage; see Figure 4.15. In other attempts of trying to maximize the efficiency, different variables were changed. The threshold on the MAD chip was constantly adjusted because it was unsure what value this should be set at. The scintillators were repositioned at different locations on the chamber in attempt to maximize the efficiency. Copper plates were added above and below the MAD card in attempt to shield the MAD chip from any noise that may affect measurements, Figure 4.16. However, after several attempts, the efficiency seemed to fall below the desired and expected value of 99%. Yet, the uncertainty that the chamber was still "picking" up noise as well as the chamber was not at the operating voltage remained. However, pushing the voltages higher was not possible since values of current were too dangerous for the chamber.

Voltage (kV)	Wire Rate	Efficiency
3400	207/501	(41.3 ± 2.2)%
3450	579/893	(64.8 ± 1.6)%
3500	360/443	(81.3 ± 1.9)%

Table 4.5: This data table contains the measured wire rates and efficiency at a particular voltage while using the ^{90}Sr source. It was observed that the wire efficiency increased as the voltage was increased.

Voltage (kV)	Wire Rate	Efficiency
3460	189/215	(87.9 ± 2.2)%
3475	244/279	(87.4 ± 1.8)%
3500	243/255	(95.3 ± 1.3)%

Table 4.6: This data table contains the measured wire rates and efficiency at a particular voltage while using cosmic rays. It was observed that the wire efficiency increased as the voltage was increased.

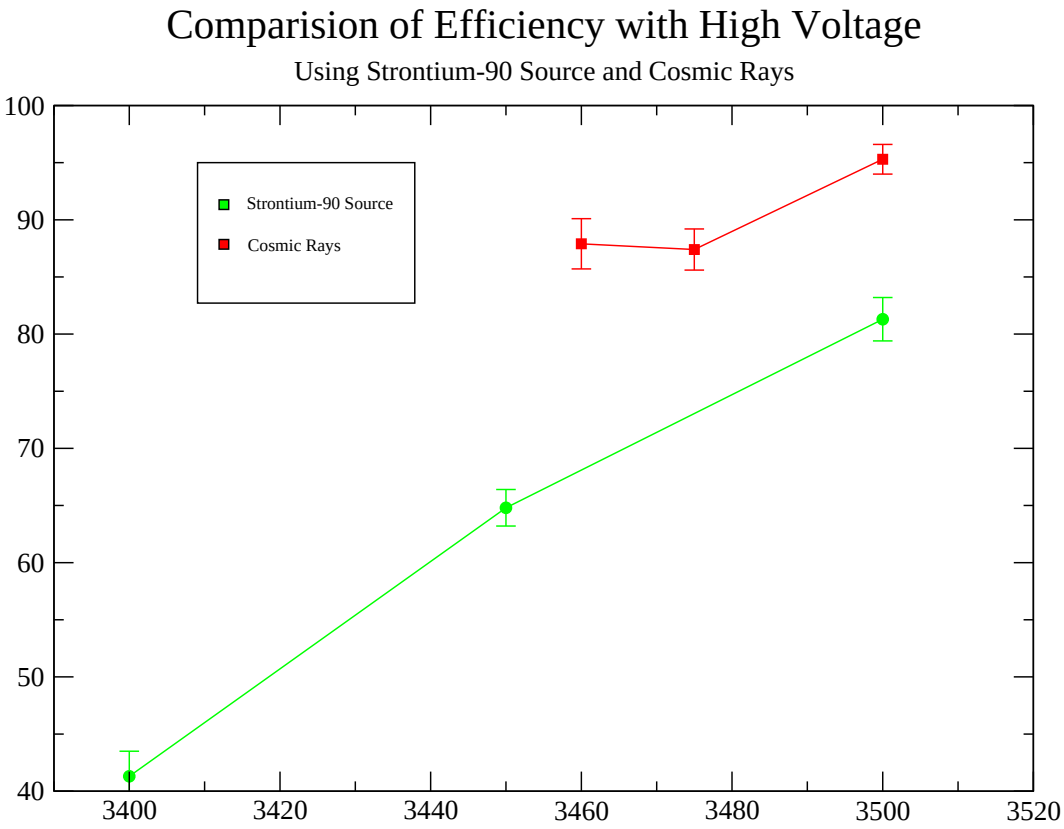

Figure 4.15: This plot illustrates a comparison of the the efficiency for the chamber with respect to the high voltage applied. One efficiency (green) was measured using the ^{90}Sr source, while the other efficiency (red) was measured using cosmic rays. The efficiency measured with the cosmic rays appears to be better than that of the efficiency measured with the ^{90}Sr source. Also, as voltage is increased, it is observed that the efficiency increases. This suggests that higher voltages are needed to obtain the desired operating point. However, the efficiencies in this plot are higher than reality because it was suspected that the data was "poisoned" by false triggers.

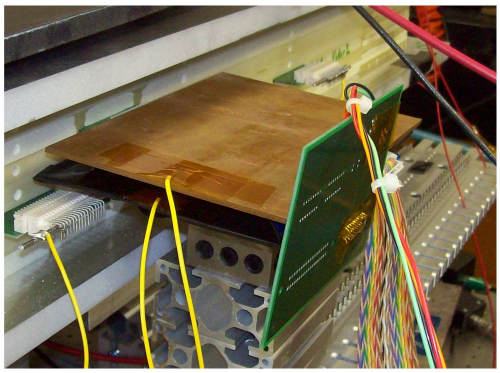

Figure 4.16: This photo shows the copper plates that were used to shield the MAD card. This shielding was important because it limited the noise that was being picked up by the MAD card.

It appeared that this first chamber would require more diagnostic work before understanding the properties of the chamber. Since higher voltages could not be applied to the chamber due to the spiking current, it was decided to pinpoint where in the chamber the current was coming from. To do this, an ammeter was connected to each individual readout card on the top and bottom wire frames and the current was measured with a voltage of 3480V. The total current drawn by the chamber at this voltage was 38μA, with 36.3μA being drawn from the bottom chamber and 0.4μA from the top. A plot of the currents drawn by each readout card was made (Figure 4.17). Most of the current was being drawn from the bottom wire frame, with 11^{th} readout card drawing the most current on this bottom frame. It was thought that the cause for the bottom wire frame drawing the most current could be due to height or separation distance variations in the individual wires along this frame. However, instead of spending more time diagnosing the problem with this wire frame, we decided to replace the wire frame with another, which required the chamber to be disassembled. Testing of the chamber with this new wire frame in place will resume after the chamber is reassembled.

4.1 Conclusions and Future Plans

Although many problems were encountered while trying to measure an efficiency of the chamber, much had been learned. First, the bubbler effectively administers the gas mixture to the chamber, without allowing any outside gas to enter. With a broken or missing wire, the chamber is not able to reach the voltages that it should because the chamber draws large amounts of current. It was confirmed with the GARFIELD simulations that the cause of this resulted from large electric fields between the adjacent wires of the broken wire. For these Vertical Drift Chambers, it is believed, when using the Argon/Ethane/CO_2 gas mixture, that the operating voltage

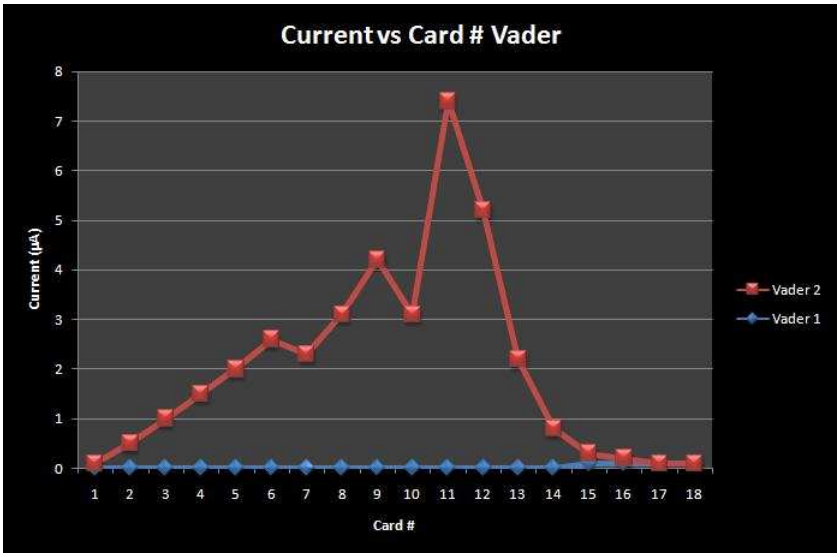

Figure 4.17: This plot shows that the bottom wire frame (VADER 2) draws a significant amount of the current that the entire chamber is drawing. Instead of trying to diagnoise the problems with this bottom wire frame, it was decided to replace the bottom frame with another wire frame and resume testing of the chamber. Note: Card #10 on this plot has fewer connected wires than the other readout cards and therefore it would be expected that the current would less than if it had contained all 16 wires.

is near 3.4kV. Also, in order to properly condition the chamber, it takes roughly 24-48 hours of applying high voltages (in step increments). The chamber does see different cosmic rays and events related to the ^{90}Sr source. The MAD card works properly; however, it is important to shield this card since it is sensitive to background noise in the laboratory. An efficiency of the chamber was not able to be measured precisely due to problems that were experienced with noise in the electronics and the currents drawn by the chamber.

In terms of future work, there is still quite a bit of work left to complete. With the wire frame replaced, the chamber will need to be reassembled and conditioned, which should be completed within a week. During conditioning, higher voltages will be tested in order to see if the current drawn by the chamber has decreased. It is hoped that the current will decrease so that higher voltages can be used when measuring the efficiency of the chamber. After conditioning, the efficiency of the chamber will be tested in the same way, using cosmic rays and the ^{90}Sr source. Once the efficiency of the chamber has been measured and it is at or near 100% efficiency, construction of the next chamber will take place and the process of conditioning and measuring the efficiency will be repeated until all 5 vertical drift chambers have been constructed, tested and characterized.

Bibliography

[1] B.R. Martin, G. Shaw. Particle Physics. John-Wiley and Sons Ltd, 1992. Ch. 8. pp 192-230.

[2] Rudolf Janoschek, Chirality- From Weak Bosons to the- Helix. Springer-Verlag, 1991. pp 2-12.

[3] G.H. Wagniere. On Chirality and the Universal Asymmetry, Reflections on Image and Mirror Image. VHCA, 2007. pp 24-27.

[4] L.H. Ryder. Elementary Particles and Symmetries. Gordon and Breach Science Publishers, 1986. pp. 136-140.

[5] W.T.H. Van Oers, The Qweak Experiment: a Search for New Physics at the TeV Scale. Nucl. Phys. **805**. 2008. 329c-337c.

[6] Armstrong et al. The Qweak Experiment: A Search for New Physics at the TeV Scale Via the Measurement of the Protons Weak Charge. http://www.jlab.org/qweak/. 2001. (Unpublished; Proposal to Jefferson Lab Program Advisory Committee).

[7] Brian P. Walsh. W&M Senior Thesis Project: "Development of a Flatness Scanner and Simulation for Qweak Wire Chambers". 2007. (Unpublished)

[8] W. Blum, L. Rolandi. Particle Detection with Drift Chambers. Springer-Verlag. 1994. pp 1-8.

[9] S.C. Bennett and C.E. Wieman, Phys. Rev. Lett. 82, 2484 (1999); C.S.Wood, et al., Science 275, 1759 (1997).

[10] P.L. Anthony, et al., (SLAC E158 Collaboration), Phys. Rev. Lett. 95, 081601 (2005).

[11] G.P. Zeller, et al., (NuTeV Collaboration), Phys. Rev. Lett. 88, 091802 (2002).

[12] Veenhof, Rob. "Garfield, a drift-chamber simulation program User's Guide, Version 4.29". http://www.slac.stanford.edu/comp/physics/cernlib/cerndoc/garfield.ps.gz. Version 4.29. 30 Nov 1993.